DOI: https://doi.org/10.46354/i3m.2019.imaaca.016

# COMPARISON OF TRAJECTORY TRACKING AND OBSTACLE AVOIDANCE STRATEGIES FOR A MULTI-AGENT DYNAMIC SYSTEM

**Martín Crespo[a,b], Matías Nacusse[a,b], Sergio Junco[a]**

[a] Laboratorio de Automatización y Control (LAC), Departamento de Control, FCEIA, UNR. Rosario, Argentina
[b] CONICET: Consejo Nacional de Investigaciones Científicas y Técnicas. Argentina

[a] crespom@fceia.unr.edu.ar, nacusse@fceia.unr.edu.ar, sjunco@fceia.unr.edu.ar

**ABSTRACT**

This paper designs different laws for formation control and obstacle avoidance for a group of robots with holonomic dynamics and presents a set of simulations that validate and compare them. The Bond Graph methodology, used to design the control laws, together with the physical interpretation of both the obstacles and the interaction between the robots, allows addressing the problem with an energy-based approach. A multi agent scheme is proposed where a leader drives a formation of agents through a desired path. The formation is organized in different hierarchy levels and the control laws for the robots arise from considering the interaction among them through virtual dampers and springs. Two different techniques are addressed for collision avoidance and three scenarios are presented to test the different techniques for coordinated tracking and obstacle collision avoidance. Simulation results are presented to show the good performance of the control system.

Keywords: formation control, obstacle avoidance, energy based methods, bond graphs.

## 1. INTRODUCTION

In the last decades the lower prices of the robots made feasible the utilization of large number of robots for several tasks such as surveillance, search and rescue or data acquisition. The problem of formation and movement in specified geometrical shapes has been widely studied.

The concept of coordinated tracking is an extension of the widely known problem of trajectory tracking (Egerstedt & Hu, 2001). That is, the objective is to find a coordinated control scheme for a group of robots that maintaining a desired scheme of formation could perform a desired task as a group.

This paper tackles the problems of Formation Control and Vehicle Following control (A. & H., 2018) for a group of holonomic vehicles which are represented as masses in the plane.

These problems were treated in the literature with multiple approaches, depending on the sensing capabilities of each agent and the desired topology, to mention: Leader Following, Predecessor-Following (also known as unidirectional connection), Leader-Predecessor follower, Predecessor-Successor (also known as bidirectional connection), etc. The reader must refer to (A. & H., 2018), (Zhang Z. & L., 2016), (R. & J., 2010), (S. & R., 2013) for a sound review of these topologies and others.

This paper uses a hierarchical unidirectional interconnection structure where each agent receives information about the relative position and the velocity of some of its surrounding robots. The robot acts as if it were connected with a spring and a damper with the surrounding agents but the reaction force of this interconnection may not affect the other agents.

Two interconnection structures are defined to generate multiple configurations. In the first one, called Scheme A, the agent receives information of only two surrounding robots, one from a superior level of hierarchy and the other from the same level. In the second scheme, called Scheme B, the robot receives information of four agents, two from a superior level of hierarchy and the others from the same level.

The problem of obtaining the obstacle avoidance law inspired in a physical phenomenon have been addressed in (Rezaee & Abdollahi, 2013) where each robot is modeled as an electric charge.

Several papers present obstacle avoidance approaches based on the artificial potential field concept (Khatib, 1986) (Alvarez D. & R., 2003). In (Matoui, Boussaid, & Abdelkrim, 2018) an attractive and a repulsive potential force are proposed to pull the robot toward the intended goal and to repel the robot from the zone of the obstacles, respectively, for real time obstacle avoidance. However, those methods suffer from points of local minima at which the robots become trapped. In (Park, Jeon, & Lee, 2001) a potential field approach with simulated annealing is proposed to avoid local minima. (Yun & Tan, 1997) proposes a switching control algorithm to avoid local minima. Even if successful, such kind of methods includes extra computation and is intrinsically less satisfactory than a method which avoids local minima from the outset (Graham & Buckingham, 1993).

The method proposed in (Connolly, Burns, & Weiss, 1990) utilizes a potential field characterized by a function that satisfies Laplace's Equation under

Dirichlet boundary conditions. The generated potential field does not contain any local minima over the region. The above techniques are presented mainly for the control of robot manipulators for both, obstacle avoidance and joint control in the case of redundant manipulators. Several other works propose potential fields for the coordination and obstacle avoidance of multi robots systems (Cai, Yang, Zhu, & Liang, 2007) (Leonard & Fiorelli, 2001).

The physical approach used here for both, formation control and obstacle avoidance call for multi-domain modeling frameworks. Besides the traditional Euler-Lagrange approach to modeling and control in robotics (Siciliano, Sciavicco, Villani, & Oriolo, 2010), the Bond Graph (BG) technique (Karnopp, Margolis, & Rosenberg, 2000) is increasingly gaining space as it is capable of representing the virtual interaction between the robots and the obstacles, very useful for analysis and simulation. The BG approach also provides methods to design control laws for physical systems (S. J. , 2004), (Dauphin-Tanguy G. & C., 1999).

The paper is organized as follows: in Section 2 the problem formulation is stated. Section 3 presents the solution to the formation control problem. In Section 4 two different control laws are designed to avoid obstacle collision of holonomic robots. In Section 5 simulation data is provided to illustrate the main results presented in the above sections. Finally, Section 6 draws some conclusions and provides future directions of research.

## 2. PROBLEM FORMULATION

The purpose of this paper is to present and compare different control strategies for a group of holonomic robots that ensure on the one hand a coordinated displacement from a starting location to a desired goal position and, on the other, obstacle collision avoidance. In the following sections three strategies are presented addressing these problems with different approaches. A control law that keeps the robots in a desired formation is common to all the three strategies. The objective of this common control law is to make the robots converge to the formation and to follow a robot leader while maintaining the stability of the formation.

### 2.1. First Strategy

In this strategy a rejection force based on a spring principle is proposed for obstacle avoidance. The control of the formation movement is done through a trajectory tracking control law applied to the leader robot.

### 2.2. Second Strategy

In this case, a control law based on a potential function is implemented in order to both avoid obstacle collision and drive the formation to the final position. The proposed potential function, that models the obstacles and the goal position with high and low values, respectively, satisfies the Laplace's equation in all the workspace. In that way, the gradient of the function drives the robots toward the goal while avoiding the obstacles.

### 2.3. Third Strategy

This strategy implements an obstacle avoidance law that results from modeling only the obstacles with a potential function. For its part, the movement of the formation is controlled by a trajectory tracking control law applied to the leader.

## 3. FORMATION CONTROL

In this section the formation control problem is presented as a coordinated tracking problem where the objective is to drive a group of robots in the plane while keeping a specific formation.

The formation, depicted in Figure 1, is composed by one leader and $n$ agents organized in hierarchical levels. A pyramidal topology with a mesh of identical triangles is shown, but this does not imply a loss of generality as any other form can be specified through the adequate choice of the length of the triangles sides. The directions of the arrows represent the flow information that the robots exchange each other.

Thus, given a desired trajectory for the leader, the objective for the agents is to converge to the formation and to follow the leader while maintaining the stability of the formation and avoiding obstacle collision.

Notice that in the stationary state, with the leader located in its final position, the agent's formation may adapt any orientation around the leader. In this work, global orientation of the formation will not be controlled.

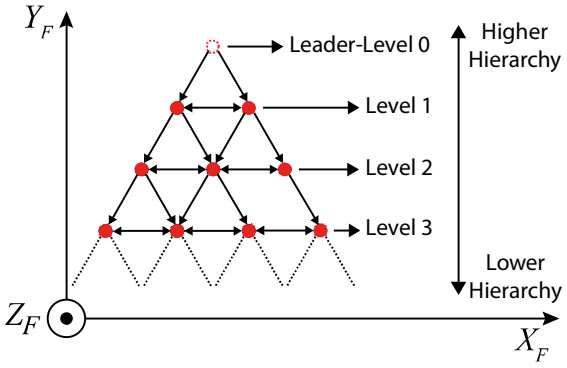


Figure 1: Interconnection network of the desired formation.

The control of the desired formation scheme is achieved through a decentralized and hierarchical architecture where each agent has its own control law. As the robots have holonomic dynamics, they may be treated as point masses. Thus, the dynamics of both the leader and the agents is simply given by $m\ddot{q} = u$, where $q = [q_x \; q_y]^T$ denotes the position of the robot in the plane and $u \in \mathbb{R}^2$ is the control force vector expressed in Cartesian coordinates of an inertial reference system. The action exerted by the controller on the leader is

$$u_L = F_T + F_O \quad (1)$$

where $F_T$ and $F_O$ represent the trajectory tracking control law and the obstacle avoidance force, respectively. In the case of the agents the control law of the robot is characterized by

$$u_A = F_c + F_O \quad (2)$$

where $F_c$ and $F_O$ represent the convergence to the formation and the obstacle avoidance force of the agent, respectively.

This section deals with obtaining the feedback law $F_C$ for the formation control of the agents.

Each agent interacts with agents that belong to the same level of hierarchy and with those from the superior hierarchy. The proposed topology is of the type Predecessor-Following where the agents that belong to Level $j$ receive position and velocity information from agents of level $j-1$ and are power coupled with those from Level $j$.

Taking into account the above idea, two kinds of interaction schemes arise considering the interconnection network of the formation shown in Figure 1. In the first one (Scheme A which corresponds to the agents on the periphery of the formation) the agent interacts with two other agents, one belonging to the same hierarchy level and the other to the superior level. In the second one (Scheme B which corresponds to the agents in the interior of the formation) the agent interacts with other four agents, two belong to the same hierarchy level and the other two to the superior one.

The control law for each agent comes from considering a virtual damper-spring connected between the agent and its interacting partners, as explained in the next sections. BG models of the formations are constructed ad hoc to obtain the control laws of the agents.

### 3.1. Scheme A

Consider an agent of Level $j$ in the scheme A of interaction. As mentioned above, the agent interacts with two other agents as shown in Figure 2-a.

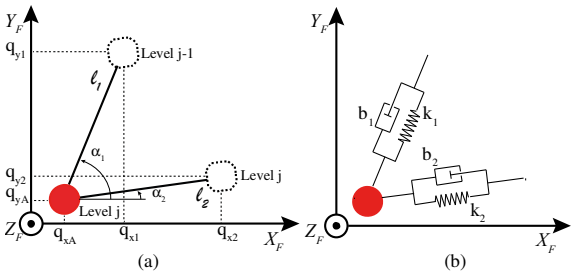


Figure 2: Scheme A - (a) Geometric variables (b) Schematic diagram.

The schematic diagram in Figure 2-b shows the virtual dampers and springs connected with its two interacting agents. The formation control vector $F_C$ for a peripheral agent, the red one at level $j$ in Figure 2 for instance, arises from considering the virtual BG shown in Figure 3. There, sub index $i = 1$ indicates the agent in level $j-1$, while sub index $i = 2$ indicates the agent at the same level $j$. Notice that a dissipation term is added to the movement of the agents in the plane.

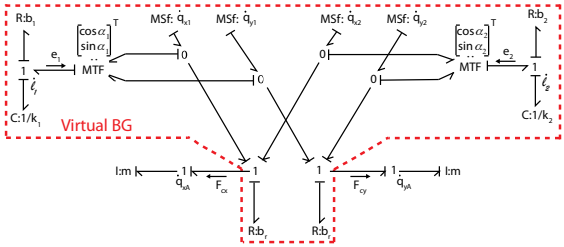


Figure 3: Scheme A – Virtual BG model.

The resulting control law is

$$F_c = \begin{bmatrix} F_{cx} \\ F_{cy} \end{bmatrix} = \begin{bmatrix} e_1 c_1 + e_2 c_2 - b_r \dot{q}_{xA} \\ e_1 s_1 + e_2 s_2 - b_r \dot{q}_{yA} \end{bmatrix} \quad (3)$$

where $b_r$ is the friction coefficient assigned to the movement of the agents in the plane, and $s_i$ and $c_i$ stand for $\sin\alpha_i = \frac{q_{yi} - q_{yA}}{l_i}$ and $\cos\alpha_i = \frac{q_{xi} - q_{xA}}{l_i}$, respectively for $i = 1,2$. The forces with the interacting agents are

$$e_i = k_i(l_i - l_{noi}) + b_i \dot{l}_i \quad (4)$$

where $k_i$ and $b_i$ are the spring and damper coefficients of the interaction $i$, respectively. The distances between the agents are

$$l_i = \sqrt{(q_{xi} - q_{xA})^2 + (q_{yi} - q_{yA})^2} \quad (5)$$

And $l_{noi}$ the natural length of the spring of the $ith$ interaction. These lengths determine the topology of the mesh defining the geometric layout of the formation. The expression for $\dot{l}_i$ is

$$\dot{l}_i = cos\alpha_i(\dot{q}_{xi} - \dot{q}_{xA}) + sin\alpha_i(\dot{q}_{yi} - \dot{q}_{yA}) \quad (6)$$

### 3.2. Scheme B

Consider an agent of Level $j$ in the scheme B of interaction. As mentioned above, the agent interacts with other four agents as shown in Figure 4.


ISBN 978-88-85741-31-7; Bruzzone, Dauphin-Tanguy and Junco Eds

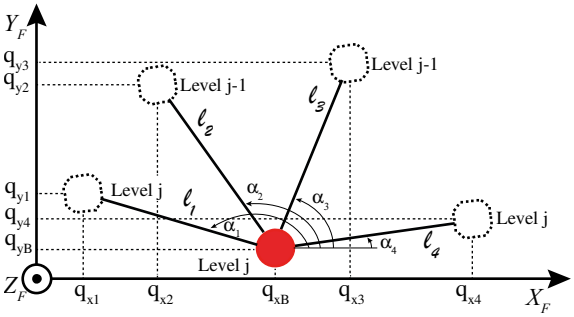


Figure 4: Scheme B - Geometric variables.

The distances $l_i$ between the agents are

$$l_i = \sqrt{(q_{xi} - q_{xB})^2 + (q_{yi} - q_{yB})^2} \tag{7}$$

while the forces $e_i$ are the same as (5). The expression of $\dot{l}_i$ yields

$$\dot{l}_i = cos\alpha_i(\dot{q}_{xi} - \dot{q}_{xB}) + sin\alpha_i(\dot{q}_{yi} - \dot{q}_{yB}) \tag{8}$$

The schematic representation of the Scheme B is shown in Figure 5.

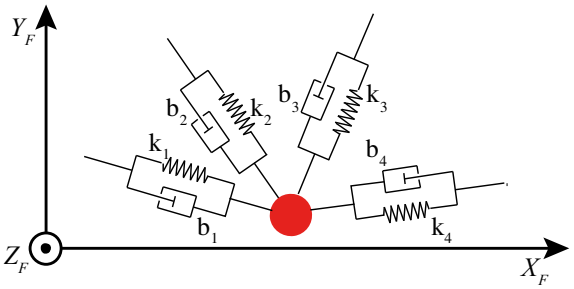

Figure 5: Scheme B - Schematic diagram.

In a similar way to scheme A the control vector $F_c$ of the agent of scheme B, is obtained from the virtual BG depicted in Figure 6

$$F_c = \begin{bmatrix} F_{cx} \\ F_{cy} \end{bmatrix} = \begin{bmatrix} e_1c_1 + e_2c_2 + e_3c_3 + e_4c_4 - b_r\dot{q}_{xB} \\ e_1s_1 + e_2s_2 + e_3s_3 + e_4s_4 - b_r\dot{q}_{yB} \end{bmatrix} \tag{9}$$

where $b_r$ is a friction coefficient, $c_i = \frac{q_{xi} - q_{xB}}{l_i}$, and $s_i = \frac{q_{yi} - q_{yB}}{l_i}$ for $i = 1, \cdots, 4$.

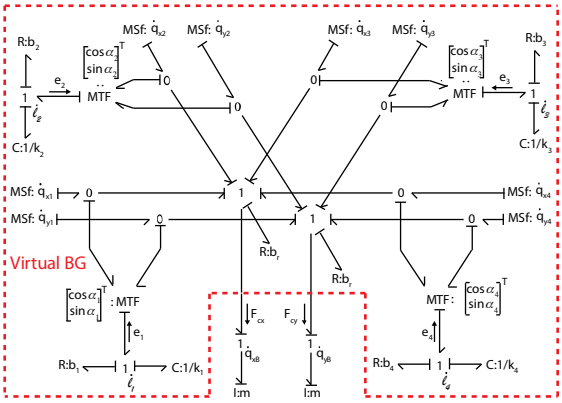


Figure 6: Scheme B - Bond Graph model.

Notice that the agents belonging to the same hierarchical level are power coupled. That is, the force of the link that joins two agents of the same level is the same and is computed by and applied to both of them.

## 4. OBSTACLE AVOIDANCE & NAVIGATION

In this section the avoidance of both static and dynamic obstacles is addressed presenting two different techniques. The first one considers a repulsion force via a spring-damper based approach. The work (J. & Y., 1989) proposes a repulsive force for obstacle avoidance. In the second one the movement of the agents is inspired in the flow of a river in a valley. Thus, the workspace is modeled with a potential function where high values of potential are assigned to the obstacles (Connolly C. & R., 1990). Both techniques define the obstacle avoidance force $F_O$ presented in (1) and (2) of the individual control laws of both, the leader and the agents, respectively.

Notice that in the former technique, the information about the obstacle becomes known to the robot through sensors during run-time whereas for the latter, the obstacle information is supposed to be known by the robot entirely before. This allows for considering dynamic obstacles in the first technique.

### 4.1. Spring-damper based approach

First the study of the obstacle avoidance problem is treated by means of a virtual spring-damper technique. This technique consists on applying a force to the center of the robot to move it away from the obstacle. The force is inversely proportional to the distance between the robot and the obstacle, and can be interpreted as the reaction force of a virtual spring attached to the obstacle and the center of the robot as shown in Figure 7-a. The virtual damper has been added to avoid oscillations during the rejection of the robots.


ISBN 978-88-85741-31-7; Bruzzone, Dauphin-Tanguy and Junco Eds

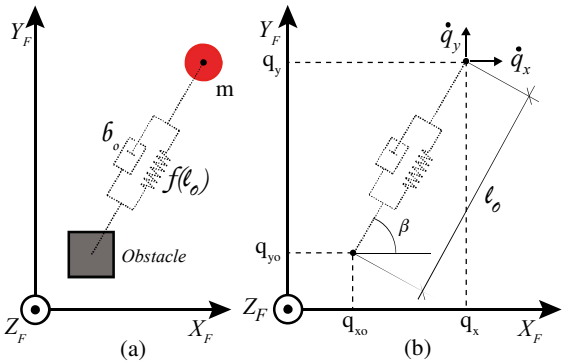

Figure 7: (a) Schematic diagram (b) Geometric variables.

The distance $l_o$ between the robot and the obstacle can be computed as

$$l_o = \sqrt{(q_x - q_{xo})^2 + (q_y - q_{yo})^2} \tag{10}$$

where $q_{xo}, q_{yo}$ represent the position of the obstacle in the plane as depicted in Figure 7-b. The force of the virtual spring as a function of the distance $l_o$ is chosen as

$$f(l_o) = \frac{k_o}{l_o^3} - \mu_F \tag{11}$$

where $k_o$ is the spring constant and $\mu_F$ a positive constant value that allows negative excursion of the function $f(l_o)$ as shown in Figure 8-a. In this way, for distances $l_o$ greater than

$$R_F = \sqrt[3]{k_o/\mu_F} \tag{12}$$

the force exerted by the spring is negative. This means that beyond a circumference of radius $R_F$ centered in the obstacle the virtual spring exerts an attraction force to the robot.

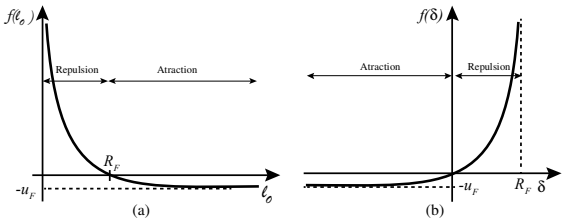

Figure 8: Avoidance function around the obstacle.

Even if in principle it is expected that the force applied to the agent by the spring vanishes as the robot moves away from the obstacle, it will be seen that this behavior allows treating the spring as a passive component. In fact, considering the change of coordinates $\delta = R_F - l_o$, equation (10) leads to

$$f(\delta) = \frac{k_o}{(R_F - \delta)^3} - \mu_F \tag{13}$$

This new function is evaluated in the first and third quadrant as shown in Figure 8-b. In that way, the addition of the term $\mu_F$ in the avoidance function and the change of coordinates ensure the passivity of the virtual spring component. The value that is assigned to $\mu_F$ is low and plays a secondary role.

**Remark:** *Notice that in an physical implementation the virtual spring may never work in traction since the sensing range of the sensors implemented in the robots is limited.*

Finally, reading the virtual BG shown in Figure 9, the implemented obstacle avoidance force vector $F_o$ is

$$F_o = \begin{bmatrix} cos\beta \\ sin\beta \end{bmatrix} \left(f(\delta) + b_o\dot{\delta}\right) \tag{14}$$

and, considering a static obstacle

$$\dot{l}_o = cos\beta\,\dot{q}_x + sin\beta\,\dot{q}_y \tag{15}$$

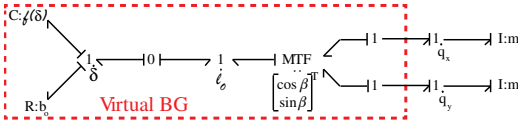

Figure 9: Virtual Spring – Bond Graph model.

However, as in (1) the force applied to the leader consists on the sum of two control laws obtained through different methods, the leader could be affected by local minima, becoming trapped in a position different from the final desired one. In this sense, to avoid local minima, an artificial potential method is presented.

### 4.2. Artificial potential

This method proposes a model of the environment in which each obstacle exerts a repulsive force while the goal position exerts an attractive force.

In this way a virtual potential field is generated in all the workspace. High and low values are assigned to the obstacles and goal position, respectively. As the generated field satisfies the Laplace's Equation under Dirichlet conditions, the resulting field is continuous in all the workspace and does not have any local minima (Connolly C. & R., 1990).

The generated potential field is a harmonic function $\emptyset$ in the domain $\Omega \epsilon \mathbb{R}^2$ that satisfies the Laplace's equation

$$\nabla^2\emptyset = \frac{\partial^2\emptyset}{\partial q_x^2} + \frac{\partial^2\emptyset}{\partial q_y^2} = 0 \tag{16}$$

As it can be seen if the second derivatives are not zero, the curves of the function $\phi$ must have second derivatives with opposite signs, in that way if not plane, there is always a direction where the curve increases or decreases. Thus, the function $\phi$ does not have any local minima.

Numerical solutions for Laplace's Equation can be obtained from finite difference methods (Burden RL. & AC, 1981). Consider $u\left(q_{x_i}, q_{y_i}\right)$ a discretization of the function $\phi$ in the domain $\Omega$. The second derivatives can be approximated by Taylor series as

$$\phi_{q_x q_x}(q_{x_i}, q_{y_i}) = \frac{u(q_{x_{i+1}}, q_{y_i}) - 2u(q_{x_i}, q_{y_i}) + u(q_{x_{i-1}}, q_{y_i})}{h^2}$$
$$\phi_{q_y q_y}(q_{x_i}, q_{y_i}) = \frac{u(q_{x_i}, q_{y_{i+1}}) - 2u(q_{x_i}, q_{y_i}) + u(q_{x_i}, q_{y_{i-1}})}{h^2} \quad (17)$$

Where $h$ is the step size to approximate the derivative. As $\phi$ satisfies the Laplace's Equation, $u\left(q_{x_i}, q_{y_i}\right)$ is expressed by

$$u(q_{x_i}, q_{y_i}) = \frac{u(q_{x_{i+1}}, q_{y_i}) + u(q_{x_{i-1}}, q_{y_i}) + u(q_{x_i}, q_{y_{i+1}}) + u(q_{x_i}, q_{y_{i-1}})}{4} \quad (18)$$

To obtain the values of the harmonic function $\phi$ in the discretized points of the grid, the linear system is solved through iteration using the Gauss-Seidel method. This method consists in replacing repeatedly each element of the grid, using an iterative method, by the average of its adjacent elements. The boundary conditions are introduced specifying the values of the function $u\left(q_{x_i}, q_{y_i}\right)$ at the boundary of the domain $\partial\Omega$ (Dirichlet boundary conditions) and remain fixed.
The gradient of the potential function $\emptyset$ determines the vector force $F_o$ that keeps away the robots from the obstacles and conducts them toward the goal.

$$F_o = \begin{bmatrix} \nabla_{q_x} \emptyset \\ \nabla_{q_y} \emptyset \end{bmatrix} \quad (19)$$

In this case the leader, and consequently the formation, moves toward the goal through a path determined by the gradient descent method. In this way, none tracking force is used in the control law of the leader, so that (1) becomes

$$u = F_O \quad (20)$$

As can be noticed, $F_o$ not only serves as an obstacle avoidance force in (2), in this case also conducts the agents toward the goal. Thus, the driving forces of the agents come not only from the formation control law but also from the obstacle avoidance force.

## 5. SIMULATION

In this section, the performance of the different strategies is assessed via simulations performed in the 20 Sim environment (20-Sim, Version 4.4, 2014).
In the simulation set $n = 5$ agents have been considered and, with the leader, all are distributed in three hierarchical levels.
The desired trajectory of the leader shown in Figure 10 starts at $(q_x, q_y)$ = (1,1) and finishes at $(q_x, q_y)$ = (9,9). As it can also be seen in Figure 10, the obstacle is a square of $(1m \times 1m)$ whose center is located at $(q_{xo}, q_{yo})$ = (3.5,3.5). The formation, with the robots in their initial positions shown in Figure 10, is composed by the leader-Level 0 (red) and five agents distributed in Level 1–Level 2 (blue and green, respectively.)

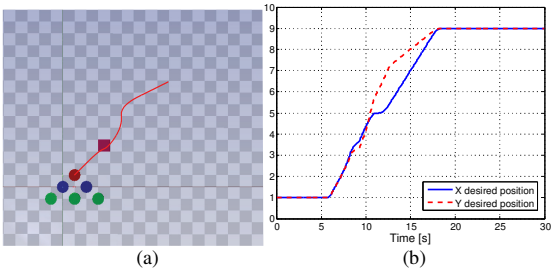


(a) (b)

Figure 10: (a) Simulated scenario - desired path, obstacle and robots (b) Desired trajectory $q_d$.

Three different strategies are tested. In the first one the implemented obstacle avoidance technique is the virtual spring-damper approach seen in Section 4.1. In the second one, the avoidance force is implemented using the technique seen in Section 4.2. Finally, in the third strategy only the obstacle is modeled through a potential field, being the avoidance force the gradient of the potential function.
The trajectory tracking law of (1) is

$$F_T = m\ddot{q}_d + \mathrm{K_D}(\dot{q}_d - \dot{q}) + \mathrm{K_P}(q_d - q) \quad (21)$$

with $K_P$ and $K_D$ positive definite (diagonal) matrices, and $\dot{q}_d$ and $q_d$ the desired velocity and position in the plane of the leader, respectively. In the second case, the tracking force is zero as explained in Section 4.2.
The mass of the robots is $m_i = 1.5\ [Kg]$. The parameters of the formation law presented in (4) are set as follows: for the first level $k_i = 20[N/m]$, $b_i = 9\ [Ns/m]$, for the second level $k_i = 200[N/m]$, $b_i = 20\ [Ns/m]$, and in both levels $l_{noi} = 2\ [m]$. The matrices of (21) are $K_P = [61, 0; 0{,}61]$, and $K_D = [193, 0; 0{,}193]$.

### 5.1. Strategy 1

The first simulation discussed is a coordinated tracking with obstacle avoidance strategy, implementing a virtual spring-damper approach as seen in Section 4.1. The parameters of (11) are $k_o = 337\ [N/m]$, $b_o = 5\ [Ns/m]$, $\mu_F = 0.1\ [N]$ and according to (12), $R_F = 15[m]$. In this way, as the robots are always located closer to the obstacle than this value, the virtual spring never attracts them.
In Figure 11, consecutive snapshots of the formation are shown. As it can be seen, the implemented approach keeps away the agents from the static obstacle.
In this case, as it is supposed that each robot measures the distance to the obstacle and computes the avoidance force (14), it is not necessary to specify the position of the obstacle in advance neither predefine the scenario workspace. This implies that, eventually, dynamics obstacles could be considered.

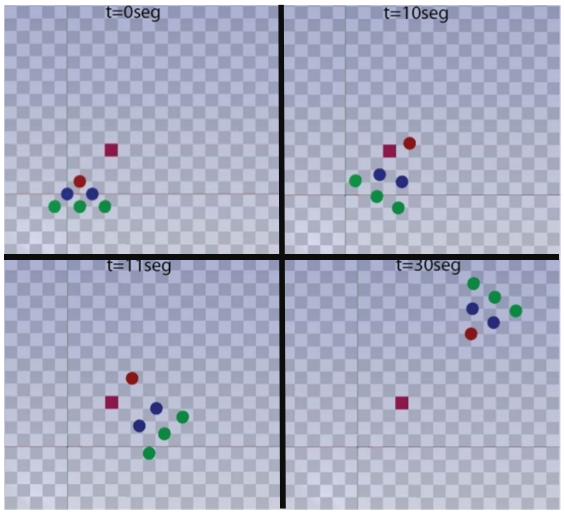


Figure 11: Strategy 1 - snapshots of the formation.

Figure 12-b depicts both, the desired and the real path travelled by the leader, while Figure 12-a shows the position error. Even if it cannot be distinguished in Figure 12-a, the final position error is not zero as, even if low, the virtual spring force is still presented when the leader arrives to its final position. This results in the agents remaining as far as possible from the obstacle, given to the formation the global orientation shown in Figure 11.

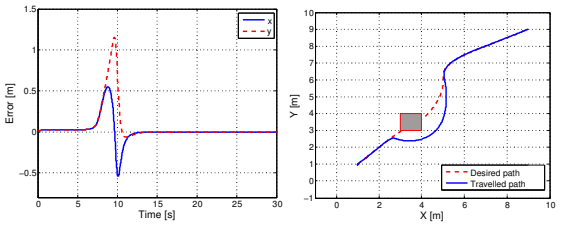


(a) (b)

Figure 12: (a) Tracking error – (b) Desired and travelled paths.

As it was mentioned above, one of the advantages of this strategy is that dynamic obstacles can be considered as it is not necessary to predefine the scenario. In that sense, under the same control strategy, a new scenario simulation was proposed in order to demonstrate this affirmation. In this scenario the static obstacle is replaced by a dynamic one that crosses the leader in his way to the goal. In this case, $\dot{l}_o$ is no longer (15), but

$$\dot{l}_o = cos\beta\ (\dot{q}_x - \dot{q}_{xo}) + sin\beta\ (\dot{q}_y - \dot{q}_{yo}) \qquad (22)$$

As it can be seen in Figure 13 all the agents avoid the obstacle, with the path done by leader depicted in Figure 14-b. The trajectory error of the leader, Figure 14-a, tends to zero with a permanent offset due to the force exerted by the virtual spring of the obstacle avoidance law.

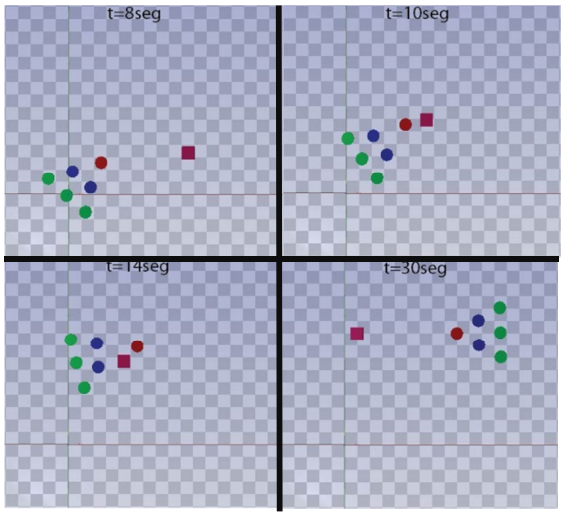


Figure 13: Strategy 1 with dynamic obstacle - snapshots of the formation.

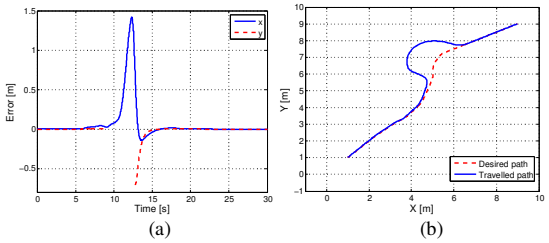


(a) (b)

Figure 14: (a) Tracking error – (b) Desired and travelled paths.

Although the implemented control seems to be successful with both static and dynamic obstacle, the leader, as explained above, may get stuck into local minima, i.e. the sum of forces in (1) may remain zero with the leader in a final position different from the desired one. To avoid this, the strategy seen in Section 4.2 is tested.

### 5.2. Strategy 2

Next, the behavior of the six robots, each operating with the collision avoidance strategy seen in Section 4.2, is tested. The graph of the potential function that satisfies the Laplace's equation is shown in Figure 15-a where the obstacle and the goal position are represented with high and low potentials, respectively. The potential function is defined in a workspace of $(10m \times 10m)$. The algorithm's flow diagram is presented in the Appendix.

In this way, as is shown in the gradient trajectory map depicted in Figure 15-b, any trajectory initiated inside the workspace converges to the goal guaranteeing the absence of any local minima.

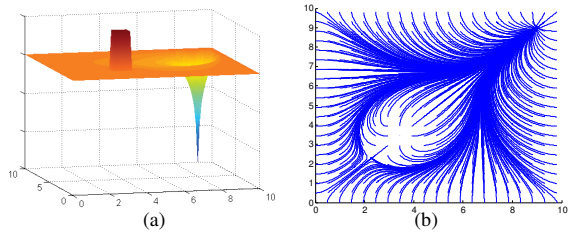
(a) (b)

Figure 15: (a) Potential function – (b) Field lines.

As mentioned above, in this case the control force $F_o$ not only assures obstacle collision avoidance but also drives the leader toward the goal as shown in Figure 16. This means that the trajectory made by the leader depends on its initial position and $F_T = 0$ in (1). Furthermore, as this control law is also applied in (2), the agents are driven to the goal not just by its interactions but also by the avoidance force $F_o$.

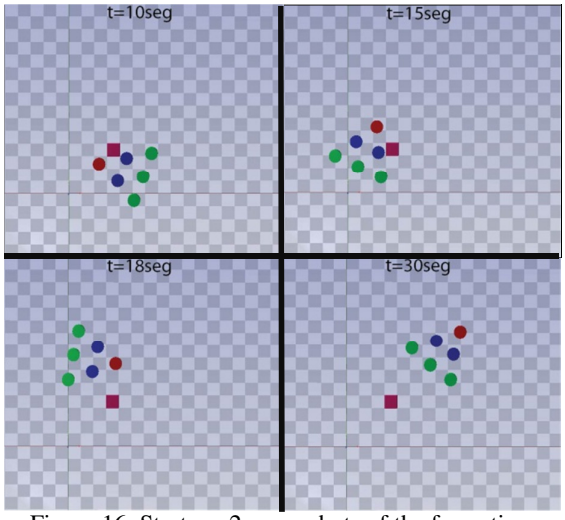


Figure 16: Strategy 2 - snapshots of the formation.

In the present case a previous study of the workspace is necessary in order to identify the position of the obstacle in advance. The final position error of the leader is zero and the global orientation of the formation remains determined by the control force $F_o$. However, desired trajectories can no longer be implemented through the control law $F_T$ and the path realized by the leader depends on its initial position.

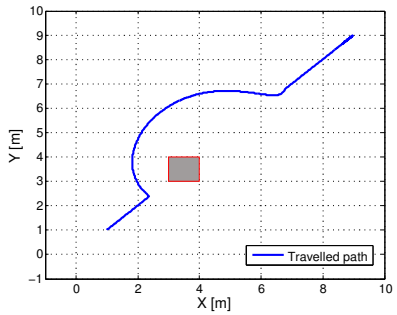


Figure 17: Path done by the leader.

To overcome this inconvenient, a third strategy is proposed in Section 5.3, where once again a potential field is created but now it only models the presence of the obstacles.

### 5.3. Strategy 3

Finally the behavior of the six robots modeling only the obstacle with a potential function is tested. The potential function that models the obstacle is depicted in Figure 18-a, and the corresponding field lines are shown in Figure 18-b.

In contrast to the previous case, the tracking trajectory law $F_T$ is given as (21). As the obstacle avoidance force vanishes beyond an area of influence, the final position error of the leader is zero.

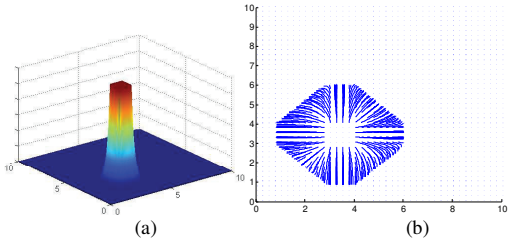
(a) (b)

Figure 18: (a) Potential function – (b) Field lines.

In the snapshots of the simulation depicted in Figure 19, it can be seen that even though the presence of the obstacle breaks the structure of the formation, the agents recover the desired interconnection once the obstacle is avoided and reach the goal with the desired formation. Notice that once the leader has reached the final position and the agents stand still, no control laws are applied to them and thus the formation can has any global orientation.

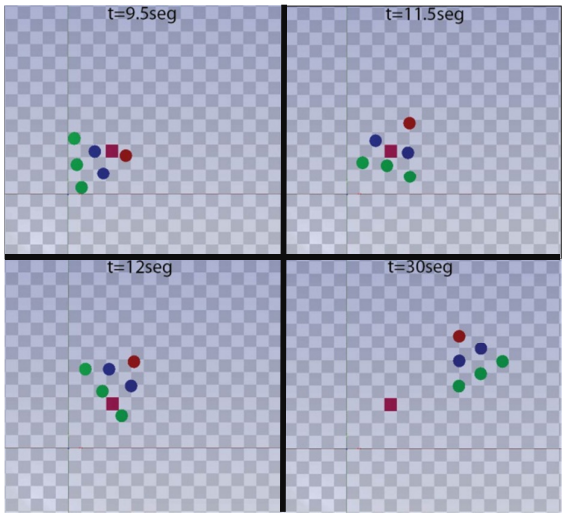


Figure 19: Strategy 3 - snapshots of the formation.

Figure 20-b depicts both, the desired and the real path made by the leader, while Figure 20-a shows the position error that is zero once the leader avoids the obstacle and reaches the final position goal.

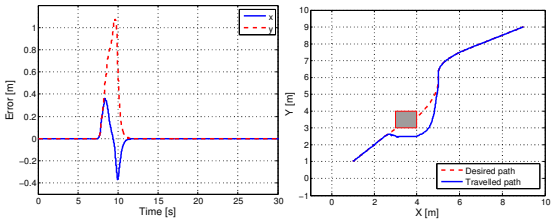


(a) (b)

Figure 20: (a) Tracking error – (b) Desired and travelled paths.

Even if in this case a predefinition of the scenario has to be done and the leader may get stuck in local minima, unlike the other two strategies, a desired trajectory can be implemented and the final position error of the leader is zero.

Also it will be demonstrated, through simulation results and considering the same strategy, how the value of the virtual springs and dampers of the control law $F_c$ of (2) affects the formation stability. Initially, whenever the hierarchy level increased, harder springs and dampers were considered. Supposing now that all the virtual dampers and springs are equal to $b_i = 9\ [Ns/m]$ and $k_i = 20[N/m]$, respectively, the formation movement of the robots can be appreciated in Figure 21. As it can be seen, even if the robots avoid the obstacle, the formation is no longer the desired one.

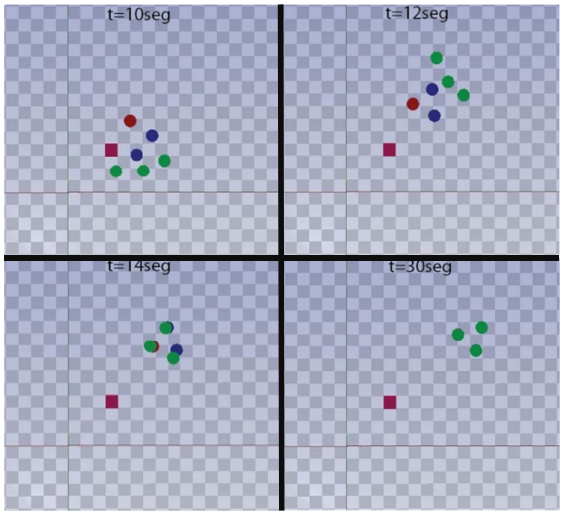


Figure 21: Strategy 3 - unstable formation - snapshots of the formation.

This happens because agents from high levels of hierarchy are subjected to higher rotational acceleration causing more instability in the formation. Even more, as the relation between the agents from different levels is unidirectional, agents from high levels does not sense position nor velocity from the lowest ones, so that the control laws do not interpret the changes in the formation as an error.

## 6. CONCLUSION

The problem of trajectory tracking and obstacle avoidance for a group of holonomic robots has been studied. The laws for formation control and obstacle avoidance have been obtained inspired on physical interpretations of the problem. Thus, the implemented control laws resulted in continues functions without commutation which implies less computation times.

Different variables have been analyzed in the simulations to study the advantages and disadvantages of each strategy: final position error of the leader, presence of local minima, formation orientation, trajectory tracking and previous analysis of the scenario.

Even if the formation was broken while it passes besides the obstacle, as shown in Section 5.3, the agents remain formed in the rest of the simulation sets and the control objectives have been achieved successfully.

Future directions include stability analysis of the formation considering different kinds of interconnections between the robots. Moreover, in order to improve the overall performance of the system, orientation control of both, the leader and the agents, will be taken into account.

## ACKNOWLEDGMENTS

The authors wish to thank SeCyT-UNR for the support to this research through the financing of PID-UNR_ING502, as well as ANPCyC for the research project PICT 2017 No 3644.

## APPENDIX

The following is the flow diagram of the iterative algorithm for the Laplace's Equation generation

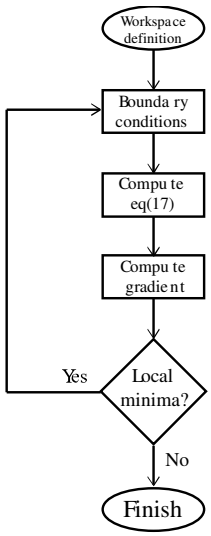


Figure 22: Laplace's equation generation.

The workspace is discretized in a mesh grid of $100x100$ equally spaced points. The definition of the Dirichlet boundary conditions consist in assigning to

the function $u(q_{x_i}, q_{y_i})$ of (18) a high value to the borders of the workspace and the obstacle and a lower value to the goal position. This ensures that, after a determinate number of iterations, all the trajectories originated among the obstacle and the border finish in the goal position. Finally equation (18) and (19) are computed, in all the points of the workspace, to evaluate function $\phi$ and its gradient, respectively.

**REFERENCES**


A., G., & R., B. (1993). Real-time collision avoidance of manipulators with multiple redundancy. *Mechatronics, 3*(1), 89-106.

A., S., & H., H. (2018). Formation Control for a Fleet of Autonomous Ground Vehicles: A Survey. *Robotics, 7*(4), 67.

Alvarez D., A. J., & R., G. (2003). Online motion planning using Laplace potential fields. *2003 IEEE International Conference on Robotics and Automation (Cat. No. 03CH37422)*, *3*, págs. 3347-3352.

Burden RL., F. J., & AC, R. (1981). Numerical Analysis." 2nd. *Ed., Prindle, Weber, and Schmidt*, 458.

Cai C., Y. C., & Y., L. (2007). Collision avoidance in multi-robot systems. *2007 International Conference on Mechatronics and Automation*, (págs. 2795-2800).

Connolly C., B. J., & R., W. (1990). Path planning using Laplace's equation. *Proceedings., IEEE International Conference on Robotics and Automation*, (págs. 2102-2106).

Dauphin-Tanguy G., R. A., & C., S. (1999). Bond graph aided design of controlled systems. *Simulation Practice and Theory, 7*(5-6), 493-513.

H., R., & F., A. (2013). A decentralized cooperative control scheme with obstacle avoidance for a team of mobile robots. *IEEE Transactions on Industrial Electronics, 61*(1), 347-354.

J., B., & Y., K. (1989). Real-time obstacle avoidance for fast mobile robots. *IEEE Transactions on systems, Man, and Cybernetics, 19*(5), 1179-1187.

Karnopp, D. C., Margolis, D. L., & Rosenberg, R. C. (2000). *System dynamics: modeling and simulation of mechatronic systems.* Wiley.

M., E., & X., H. (2001). Formation constrained multi-agent control.

Matoui F., B. B., & M., A. (2019). Distributed path planning of a multi-robot system based on the neighborhood artificial potential field approach. *SIMULATION, 95*(7), 637-657.

N., L., & E., F. (2001). Virtual leaders, artificial potentials and coordinated control of groups. *Proceedings of the 40th IEEE Conference on Decision and Control (Cat. No. 01CH37228)*, *3*, págs. 2968-2973.

O., K. (1986). Real-time obstacle avoidance for manipulators and mobile robots. En *Autonomous robot vehicles* (págs. 396-404). Springer.

Park M., J. J., & M., L. (2001). Obstacle avoidance for mobile robots using artificial potential field approach with simulated annealing. *ISIE 2001. 2001 IEEE International Symposium on Industrial Electronics Proceedings (Cat. No. 01TH8570)*, *3*, págs. 1530-1535.

R., M., & J., B. (2010). String instability in classes of linear time invariant formation control with limited communication range. *IEEE Transactions on Automatic Control, 55*(7), 1519-1530.

S., J. (2004). Virtual prototyping of bond graphs models for controller synthesis through energy and power shaping. *International Conference on Integrated Modeling and Analysis in Applied Control and Automation (IMAACA 2004).*

S., K., & R., M. (2013). Stability of two-dimensional linear systems with singularities on the stability boundary using LMIs. *IEEE Transactions on Automatic Control, 58*(10), 2579-2590.

Siciliano B., S. L., & G., O. (2010). *Robotics: modelling, planning and control.* Springer Science \& Business Media.

X., Y., & K., T. (1997). A wall-following method for escaping local minima in potential field based motion planning. *1997 8th International Conference on Advanced Robotics. Proceedings. ICAR'97*, (págs. 421-426).

Zhang Z., Z. L., & L., W. (2016). Leader-following consensus for linear and Lipschitz nonlinear multiagent systems with quantized communication. *IEEE Transactions on Cybernetics, 47*(8), 1970-1982.